Materials Today Bio 16 (2022) 100369

Contents lists available at ScienceDirect

Materials Today Bio

journal homepage: www.journals.elsevier.com/materials-today-bio

Water-driven noninvasively detachable wet tissue adhesives for wound closure

Hongjian Huang [a], Renfeng Xu [b], Peng Ni [a], Zhenghong Zhang [b,**], Caixia Sun [a], Huaying He [a], Xinyue Wang [a], Lidan Zhang [a], Ziyi Liang [a], Haiqing Liu [a,c,*]

[a] Fujian Key Laboratory of Polymer Materials, College of Chemistry and Materials Science, Fujian Normal University, Fujian, 350007, China
[b] College of Life Science, Fujian Normal University, Fujian, 350007, China
[c] Engineering Research Center of Industrial Biocatalysis, Fujian Province Higher Education Institutes, Fujian, 350007, China

A B S T R A C T

Tissue adhesive with on-demand detachment feature is critically important since it can minimize hurt to patient when it is stripped away. Herein, a water-driven noninvasively detachable wet tissue adhesive hydrogel (w-TAgel) was produced by UV-initiated radical copolymerization of N-isopropylacrylamide (NIPAM), acrylamide (AAm), gelatin methacrylate (GelMA), and urushiol. As a w-TAgel, its robust and tough mechanical property makes it suitable for dynamic wound tissue. The polyurushiol segments of it are crucial to the formation of tough adhesion interface with various wet tissues, while polyNIPAM units play an indispensable role in on-demand detachment via thermo-responsive swelling behavior because the hydrophobic aggregation among isopropyl groups is destroyed upon water treatment with temperature of 25 °C or less. Additionally, it exhibits multiple merits including good hemocompatibility, cytocompatibility as well as pro-coagulant activity and hemostasis. Therefore, our w-TAgel with strong adhesion and facile detachment is an advanced prospective dressing for wound closure and rapid hemostasis. The wet tissue adhesion and water-driven detachable mechanism may shed new light on the development of on-demand noninvasively detachable wet tissue adhesives.

1. Introduction

Tissue adhesive hydrogels (TAgels) have shown great potentials in biomedical applications such as tissue engineering [1,2], wound dressing [3–5], sensor [6,7], and human-machine interaction device etc [8,9]. However, tough adhesion of hydrogels to wet tissues is a difficult task because the hydration layer on tissue surface usually hinders interfacial interaction [10]. Additionally, facile on-demand detachment from tissue is another challenge [11]. To address the first challenge, destroying the interfacial hydration layer (IHL) through techniques like water-participated reaction and water absorption is a prerequisite for strong wet adhesion [12,13]. Inspired by wet adhesive capability of small creatures such as mussel [14,15], barnacle [16], ctenophore [17], and other marine lives [18], some tough TAgels have been developed. Particularly, gels with catechol group, which is abundant in mussel adhesive proteins (MAPs), functioning well in disruption of the IHL and creating multi-interactions on substrate surfaces [19,20], have made great contributions to tough wet tissue adhesives.

As for the second challenge, the transformation from strong adhesion to weak adhesion by triggering factors including light [21], chemical reaction [22], solvent [23], and temperature [24,25], is a principal strategy for designing on-demand adhesion-detachment adhesives. Weakening adhesion by light and chemical treatments involve in change of redox state and cleavage of disulfide bonds in adhesives [26,27]. However, exposure of UV light and chemical reagents to wound may be harmful to patients. In contrast, temperature-triggered detachment through phase transition is an ideal and easy way to remove adhesive. Recently, several on-demand detachable thermo-responsive adhesives (TRAs) have been reported [28–30]. They form adhesion at normal body temperature, while debonding as temperature changes. However, the existing on-demand detachable TRAs showed low mechanical strength, leading to hydrogel residuals left behind on tissues when it was peeled off [30]; Additionally, the adhesion strength to wet tissue is relatively low. Hence there is an urgent necessity for preparing a mechanically strong and on-demand detachable wet tissue adhesive.

Herein, we designed and prepared water-driven detachable w-TAgels by co-polymerization of N-isopropylacrylamide (NIPAM), acrylamide (AAm), gelatin methacrylate (GelMA), and urushiol (Fig. 1A). Poly(NIPAM-co-AAm-co-GelMA-co-Urushiol) (PNAGU, Fig. 1B) can strongly form adhesion to tissue and then be easily detached with the help of room temperature water. By co-polymerization with urushiol, a natural catechol compound featuring with an unsaturated long alkyl

* Corresponding author. Fujian Key Laboratory of Polymer Materials, College of Chemistry and Materials Science, Fujian Normal University, Fujian, 350007, China.
** Corresponding author.
E-mail addresses: zhangzh@fjnu.edu.cn (Z. Zhang), haiqingliu@fjnu.edu.cn (H. Liu).

https://doi.org/10.1016/j.mtbio.2022.100369
Received 5 April 2022; Received in revised form 2 July 2022; Accepted 13 July 2022
Available online 19 July 2022

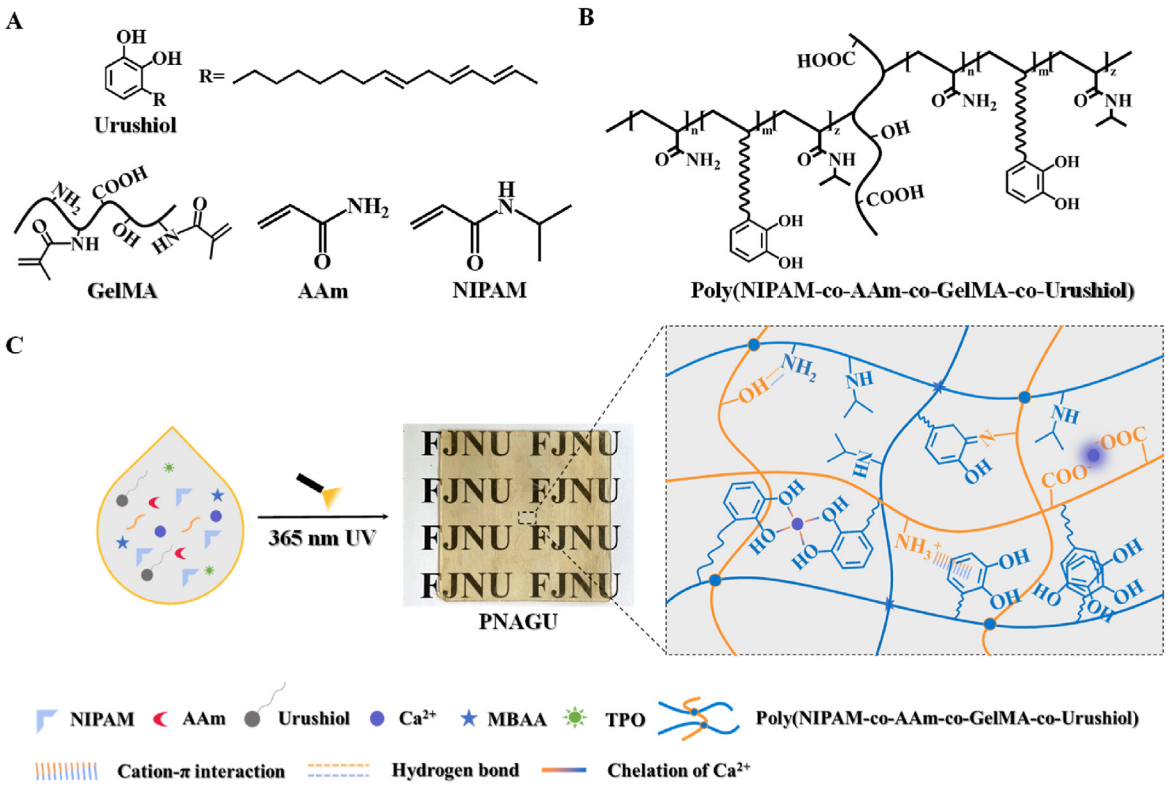

Fig. 1. Chemical structure of A) urushiol, GelMA, AAm and NIPAM, and B) Poly(NIPAM-co-AAm-co-GelMA-co-Urushiol). C) UV initiated polymerization for making a PNAGU adhesive hydrogel, and the crosslinking network in PNAGU.

chain [31], PNAGU's wet tissue adhesion is greatly enhanced because the long alkyl chain breaks the IHL and catechol group form bidentate hydrogen bonding with tissues [32]. Water-driven detachability of PNAGU is attributable to polyNIPAM segments which possessing the ability of temperature-triggered phase transition [33,34]. GelMA is a good source for biomedical materials due to its superior biocompatibility [35], while it also has been used in wound sealing for its good adhesion to tissue [36,37]. Considering the complexation ability of Ca^{2+} with COO^- of GelMA and catechol group [38,39], with pKa = 3.1 for $Ca^{2+}\cdots COO^-$ [40], and binding constant of $5.0 \times 10^8\ M^{-2}$ for one Ca^{2+} with two catechol groups [41], such physical cross-linkings are introduced for energy dissipation to improve hydrogel's toughness. It is well expected that PNAGU shows good synergetic effects of wet tissue adhesion, good mechanical property, and water-driven damage-free and harm-free detachment ("2F" detachment). Hence, PNAGU may become an ideal water-driven detachable wet tissue adhesives in some clinical applications such as wound closure and bleeding control.

2. Experimental section

2.1. Materials

Gelatin from porcine skin (type A, gel strength ~300 g bloom) and 2,4,6-trimethylbenzoyl-diphenylphosphine oxide (TPO) were obtained from Sigma-Aldrich. Methacrylic anhydride, acrylamide (AAm), and N-isopropylacrylamide (NIPAM) were obtained from Aladdin. Calcium chloride ($CaCl_2$), sodium hydroxide (NaOH), *N,N′*-methylenebisacrylamide (MBAA), sodium bicarbonate ($NaHCO_3$), sodium carbonate (Na_2CO_3), ethanol, and acetone were purchased from Sinopharm. All chemicals are analytical grade. NIPAM was purified by recrystallization to remove inhibitor before use and other reagents were used as received. Polyurethane (PU) film was bought from a local pharmacy store. Fresh porcine organs including skin, liver, kidney, heart and intestine were purchased from a local store. Chinese lacquer was bought from Institute of Lacquer, Xi'an, China, from which urushiol was extracted with ethanol. Sprague-Dawley (SD) rats with weight of ca. 200–250 g were bought from Shanghai Slack Experimental Animal Co., Ltd, China. The animal care and study followed the rules administered by the Research Animal Ethics Committee of Fujian Normal University (Protocol No. IACUC-20180013). Mouse fibroblast L929 cells were purchased from iCell Bioscience Inc (Shanghai, China) and stored at −80 °C.

2.2. Synthesis of GelMA

GelMA was prepared according to a previous method with slight modifications [42]. In detail, 5 g of gelatin was dissolved in 50 mL of sodium carbonate-sodium bicarbonate buffer (CB buffer, 0.1 mol/L, pH = 9.16) at 45 °C under stirring for 30 min, then 0.5 mL of methacrylic anhydride was added. After 1 h of reaction under dark conditions, the pH was adjusted to neutral to terminate the reaction. The reaction solution was dialyzed against deionized water at 40 °C for 7 days, and followed by lyophilization to obtain GelMA. The degree of substitution (DS) of GelMA was determined by ^1H NMR.

2.3. Preparation of poly(NIPAM-co-AAm-co-GelMA) (PNAG) hydrogel

1.6 g of NIPAM, 0.4 g of AAm, GelMA, $CaCl_2$, and 1.0 g of water were added to a beaker according to the recipe listed in Table S1, and dissolved under stirring at room temperature. Subsequently, TPO and 0.003 g of MBAA were added and stirred to dissolve into a pre-polymerization solution, which was then poured into a PTFE mold and cured under 365 nm UV light for 2 h to obtain a PNAG hydrogel with a thickness of about 500 μm.

2.4. Preparation of poly(NIPAM-co-AAm-co-GelMA-co-urushiol) (PNAGU) hydrogel

According to the recipe in Table S1, a solution containing 1.6 g of

NIPAM, 0.4 g of AAm, GelMA, $CaCl_2$, and 1.0 g of deionized water was prepared. Subsequently, certain concentration of urushiol (urushiol/monomers of NIPAM and AAm = 1, 2, and 3 wt%), TPO and 0.003 g of MBAA were added to make a pre-polymerization solution, which was then cured as described for PNAG.

2.5. ^1H NMR characterization

^1H NMR spectra of gelatin and GelMA in D_2O were characterized by Bruker 400 MHz NMR instrument. Peak area of each peak was normalized by the one at 7.3 ppm for the unreacted phenylalanine benzene ring in gelatin. The peak area of gelatin and GelMA at 2.9 ppm is coded as S_1 and S_2, respectively. The DS of GelMA is calculated using the following equation:

$$\mathrm{DS} = \left(1 - \frac{S_2}{S_1}\right) \times 100\%$$

2.6. FT-IR characterization

Nicolet-IS50 FT-IR (Thermo Fisher) was used to obtain the FT-IR spectra of dried samples in KBr form. The test range was 4000–400 cm^{-1}, and the number of scan was 32.

2.7. Phase-transition temperature of hydrogel

About 10 mg of hydrogel was weighed into a crucible and tested in a differential scanning calorimeter (DSC, Mettler) with a temperature range of 25–50 °C at a heating rate of 1 °C/min and a nitrogen flow rate of 50 mL/min.

2.8. Morphology of hydrogel

Scanning electron microscopy (SEM, Phenomenon LE) was used to observe the morphology of dry hydrogels, which were made by lyophilizing hydrogels fully swollen in 25 and 37 °C water.

2.9. Swelling behavior of hydrogel

The weight of dry sample was recorded as m_1 (g). Then the sample was immersed in deionized water at different temperatures and was removed at regular intervals. The excess water on the sample surface was dried out with filter paper and the weight of the swollen sample was recorded as m_2 (g). The swelling ratio was calculated by the following equation and the average value was reported (n = 3), and swelling ratio at 600 min was taken as the equilibrium swelling ratio (ESR).

$$\text{Swelling ratio } (g/g) = \frac{m_2 - m_1}{m_1}$$

2.10. Tensile stress-strain test

The dumbbell-shaped hydrogels (75 mm in length × 5 mm in width × 0.5 mm in thickness) were tested on a universal testing machine (LR5k, 100 N load-cell) at a speed of 50 mm/min (n = 4).

2.11. Interfacial adhesion toughness (IAT) to wet tissue

The wet porcine skin was first prewarmed at 37 °C for 30 min. Afterwards, a hydrogel (60 mm in length × 10 mm in width × 0.5 mm in thickness) was compressed onto the porcine skin for 5 s, then placed at 37 °C for 5, 10, 30, and 60 min. They were subjected to 90° peeling test (ASTM D2861) on the universal testing machine at a speed of 50 mm/min. To measure the interfacial toughness to wet tissue when treated with water of varied temperature, the adhesion interface between adhesive and porcine skin was sprayed with 25 and 37 °C water during testing. All hydrogels were backed with a PU film as a backing before testing. IAT (J/m^2) was calculated according to the following equation:

$$\mathrm{IAT} = \frac{F}{w}$$

where F (N) is the force at the platform of the curve. If there is no platform, the force at the breaking point is used; w (m) is the width of the hydrogel. Average value was reported (n = 4).

2.12. Adhesion strength to wet tissue

For simulating wound closure of two fractured tissues, wet porcine skin, liver, kidney, and heart were cut into two pieces of equal size and prewarmed at 37 °C for 30 min. A hydrogel (30 mm in length × 10 mm in width × 0.5 mm in thickness) was then used to bond the two pieces of the same kind of tissue with same adhesion area on each side at 37 °C for 30 min (Fig. 5A). Then it was tested on the universal testing machine at a shear speed of 50 mm/min. All hydrogels were backed with a PU film before testing. Adhesion strength (kPa) was calculated according to the following equation

$$\text{Adhesion strength} = \frac{F}{A}$$

where F (N) is the force at the breaking point of the curve; A (m^2) is the contact area of the hydrogel with one of the tissue. Average value was reported (n = 4).

2.13. Burst pressure of hydrogel on wet small intestine

A small hole with a diameter of 0.5 mm was made on the wet small intestine, and a hydrogel (20 mm in length × 20 mm in width × 0.5 mm in thickness) was adhered to the small intestine to seal the hole. Then it was tightly connected to a water pipe with nylon thread. Water was pumped into the pipe and the reading of the water pressure gauge was recorded when adhesion failed. Average value was reported (n = 4).

2.14. Whole blood clotting

Cotton gauze and PNAGU were placed in a centrifuge tube and prewarmed at 37 °C for 30 min 100 μL of fresh anticoagulated rat blood was then added dropwise to the sample surface and incubated for 10 min at 37 °C. 20 mL of PBS was added to the tube along the wall of the tube, and the absorbance of the supernatant at 540 nm was recorded as A_s. The absorbance at 540 nm of 100 μL of fresh anticoagulated rat blood in 30 mL of PBS was used as the reference value and recorded as A_b, and the blood clotting index (BCI) was calculated using the following equation, average value was reported (n = 4):

$$\mathrm{BCI} = \frac{A_s}{A_b} \times 100\%$$

2.15. Red blood cells (RBCs) adhesion

Cotton gauze and PNAGU were incubated in PBS at 37 °C for 1 h in centrifuge tube. The 10-fold diluted anticoagulated rat blood was added to the tube and continued incubation at 37 °C for 1 h. The sample was washed 3 times with PBS to remove non-adhered RBCs and then treated with 2.5% glutaraldehyde aq. solution at room temperature for 4 h. The sample was sequentially dehydrated with 10%, 20%, 30%, 40%, 50%, 60%, 70%, 80%, 90% and 100% ethanol/PBS solution at 10 min intervals. The sample was dried at 37 °C and then the RBCs adhesion was observed by SEM.

2.16. Platelet adhesion

Fresh anticoagulated rat blood was first centrifuged at 100 g for 10 min to obtain platelet-rich plasma. Cotton gauze and PNAGU were immersed in the platelet-rich plasma and incubated at 37 °C for 1.5 h. The treated sample was washed 3 times with PBS to remove non-adhered platelets. Subsequently, the sample was treated with 2.5% glutaraldehyde aq. solution at room temperature for 1.5 h. The sample was sequentially dehydrated with 10%, 20%, 30%, 40%, 50%, 60%, 70%, 80%, 90% and 100% ethanol/PBS solution at 10 min intervals and then dried at 37 °C for 48 h. The platelet adhesion was observed by SEM.

2.17. Hemolysis assay

Cotton gauze and PNAGU fragments were dispersed in PBS to obtain suspensions at concentrations of 0.5, 1, 2 and 4 mg/mL. They were incubated at 37 °C for 10 min, followed by adding 0.5 mL of a 10-fold diluted anticoagulated rat blood solution to 0.5 mL of the sample suspension and continued to incubate at 37 °C for 1 h before centrifugation at 100 g for 6 min. The absorbance of the resulting supernatant at 540 nm was measured and recorded as A_s. The absorbance of diluted blood in PBS and triton were recorded as A_p and A_t, respectively, using PBS and triton as negative and positive controls, and the hemolysis ratio was calculated by the following equation, average value was reported (n = 4):

$$\text{Hemolysis} = \frac{(A_s - A_p)}{(A_t - A_p)} \times 100\%$$

2.18. In vivo hemostasis

The rat liver injury model was used to evaluate the hemostatic performance of samples. Rats were randomly divided into 3 groups of 6 rats each at first. Then, 1 mL of 10% chloral hydrate was injected intraperitoneally into the rat to anesthetize it. Subsequently, the rat liver was exposed and a wound of 10 mm in length, 5 mm in depth was created on the liver. After that, cotton gauze (4 stacked layers) and PNAGU were applied onto the wound, and blood loss at 180 s was recorded. Finally, rat was euthanized by administering an overdose of 10% chloral hydrate. Average value was reported (n = 4).

2.19. Cytotoxicity assay

The mouse fibroblast L929 cells were used as a model to test the cytocompatibility of the hydrogel. Cells were cultured in a dulbecco's modified eagle medium (DMEM) with 5 mL 10% fetal bovine serum (FBS) with 5% CO_2 at 37 °C. The cell suspension was added to the 96-well plate with a concentration of 5×10^3 cells/well and cultured for 24 h with an atmosphere of 5% CO_2 at 37 °C. Then the media were removed and 100 μL of extract of hydrogel with concentrations of 0.2, 1, 5, 20, 50 mg/mL were added for 24 h and 48 h incubation. 10 μL of MTT solution (0.5 mg/mL, MedChemExpress Co., Ltd.) was added to each well and continued to incubate for 4 h. Finally, the medium was removed, followed by adding 150 μL of dimethyl sulfoxide (DMSO) and shaking for 10 min. The absorbance at 570 nm was measured, and cells without any treatment were considered as a control. The cell viability was calculated by the following equation:

$$\text{Cell viability } (\%) = \frac{A_s}{A_c} \times 100\%$$

where A_s and A_c are the absorbance of the sample and control, respectively. Average value was reported (n = 3).

The L929 cells were stained with calcein-AM and propidium iodide (PI) (Shanghai Beibo Biotechnology Co., Ltd.), then live/dead cells were observed on a confocal laser microscope (TCS SP8, Leica).

2.20. Cell growth on hydrogel

This test was according to a previous method with slight modifications [43]. Cell suspension in DMEM medium containing 1×10^5 L929 fibroblast cells were seeded on a 24-mutiwell cell culture plate, which was pre-coated with hydrogel. The plate was incubated in a CO_2 incubator at 37 °C for 3 h for cell attachment, followed by rinsing off the loosely attached cells with PBS, then 2 mL of fresh medium was added to incubate for up to 2 days. Cell proliferation was determined by Cell Counting Kit-8 (CCK8) assay for measurement of viable cell number. The assays were performed by adding 20 μL of CCK8 solution and 200 μL fresh medium to each well after aspirating the spent medium, followed by incubation at 37 °C for 3 h with protection from light. Colorimetric measurement was performed at a wavelength of 450 nm using a plate reader (BioTek Synergy). Average value was reported (n = 3). The L929 cells were stained with calcein-AM and PI, then live/dead cells were observed on a confocal laser scanning microscope (Carl Zeiss, Göttingen, Germany).

2.21. Data analysis

All experimental data were evaluated by the two-tailed unpaired *t*-test. The data are expressed as mean ± standard deviation. The statistical significance (*p* value) is defined as follows: $^*p < 0.05$, $^{**}p < 0.01$, $^{***}p < 0.001$, $^{****}p < 0.0001$.

3. Results and discussion

3.1. Preparation, characterization of hydrogels

PNAGU hydrogel was made by UV-initiated radical copolymerization of NIPAM, AAm, GelMA, and urushiol. PolyNIPAM segments contribute to the thermo-responsive phase transition of PNAGU, while polyurushiol units play a key role in improving wet tissue adhesion and mechanical properties of PNAGU [44]. The hydrogel network is cross-linked with covalent bonds and non-covalent bonds including hydrogen bonding, chelation, π-π stacking, cation-π association, and hydrophobic interaction (Fig. 1C). The reversible non-covalent interactions in the hydrogel network help energy dissipation.

^{1}H NMR spectra of gelatin and GelMA (Fig. S1) show peak signals at 5.5 and 5.3 ppm assigned to the protons of alkenyl (2H) grafted on respectively lysine and hydroxylysine units of gelatin [42]. The peak intensity at 2.9 ppm assigned to the proton of methylene (2H) on lysine, significantly decreases after reaction, indicating that most of the free amino groups of gelatin are consumed for production of GelMA. The DS of GelMA is about 90%. From FT-IR spectra of PNAG and PNAGU (Fig. S2), the superimposed peaks at 3443 cm^{-1} and 3311 cm^{-1} are assigned to stretching vibration of $–NH_2$, –NH– and –OH groups, and the peak at 2975 cm^{-1} corresponds to the stretching vibration of methylene. The peaks at 1278 cm^{-1} and 980 cm^{-1} in the spectrum of PNAGU are respectively attributable to the chelated phenolic hydroxyl group and triene group [45], demonstrating that urushiol is copolymerized with PNAG to form PNAGU. The above results indicate that PNAG and PNAGU have been successfully obtained.

3.2. Mechanical properties of hydrogels

Adhesives used for wound closure should be flexible to adapt to dynamic wounds to reduce uncomfortable sensations [46]. As described in the introduction section, Ca^{2+} in the adhesive hydrogel is mainly for enhancing hemostasis efficiency [47]. The tensile stress of PNAGs generally decreases with increasing Ca^{2+} concentration, while their strain at break varies randomly. With increasing GelMA content, the stress shows no monotonic trend, while there is a downward trend for strain (Fig. S3). Among the samples, both PNAG-6 and -11 display much better strain (190–350%) with tensile strength of ~1.30 MPa. Therefore,

their recipes were chosen for further copolymerization with urushiol to synthesize PNAGU adhesive hydrogel. In the pre-screening synthesis, it was found that the adhesive hydrogel (based on PNAG-6) had poor mechanical properties and was difficult to detach from the mold; However, the adhesive hydrogel (based on PNAG-11) showed good strength and toughness so that it could be demolded as a whole. Hence, the recipe for PNAG-11 was used to further react with urushiol to make PNAGU adhesive hydrogels for the following study.

With increasing urushiol content in PNAGU hydrogel to 3 wt%, the tensile stress decreases from 1.39 to 0.57 MPa, while the strain increases from 191.4% to 273.3% (Fig. 2A and B). In the synthesis of PNAGU, the existence of catechol group of urushiol consumes radical initiators in the polymerization [48], and we found that 4 wt% of urushiol in the precursor solution prevent polymerization from forming hydrogel even the concentration of TPO was increased to 1.0 wt%, due to it deactivates radicals by termination of the chain growth reaction. This reduction of the degree of polymerization of PNAGU results in drop of tensile stress. The strain of PNAGU could be positively affected by multi-physical interactions including hydrophobic association, π-π stacking, and cation-π interactions [44,49], which are introduced in the hydrogel network with the presence of urushiol moieties. PNAGU3 is taken as an example to demonstrate the practical deformation performance of PNAGU. It can be folded twice along the axial direction, rolled into a cylinder, and folded into a crane shape without cohesion failure (Fig. 2C–E), indicating the high plasticity of PNAGU3. The hydrogel can also be folded into a square and triangle and then be unfolded to its original shape (Fig. S4).

3.3. Swelling and morphology of hydrogels

The influence of urushiol moiety on the thermo-responsive property of PNAGU was studied by its swelling behavior and morphology of hydrogels at 37 and 25 °C. This temperature range is justified on basis of body temperature, ambient room temperature, and phase transition temperature of polyNIPAM (~33.0 °C) and PNAGU3 (~38.2 °C) (Fig. S5). ESR of PNAGU at 37 °C is smaller than that at 25 °C (Fig. 3A–C and Table S2). For example, ESR of PNAGU3 increases from 10.25 g/g at 37 °C to 15.36 g/g at 25 °C. Such a thermo-responsive swelling is attributable to the expansion of polymer chains induced by phase transition of polyNIPAM units in the hydrogel. Additionally, ESR increases with increasing urushiol content in PNAGU hydrogel. This is mainly due to easy swelling of short PNAGU chains with lower degree of polymerization when more urushiol is used in the pre-polymerization solution, since urushiol is an inhibitor of free radical polymerization.

The porous morphology of hydrogel is a more intuitive way to demonstrate the thermo-responsive swelling behavior [50]. With analysis of the SEM images and pore size (Fig. 3D and E), the enlargement in pore size of each hydrogel from 37 to 25 °C is consistent with increasing ESR. Pore size of hydrogel shows almost no increase with increasing urushiol content. Obviously, the hydrogel at 25 °C with a larger pore size confirming the thermo-responsive polymer chain expansion in the hydrogel, while the pore size at 37 °C show a contraction of hydrogel. Therefore, the change in ESR is directly related to the volume expansion of the hydrogel on a macroscopic scale.

3.4. Adhesion performance to wet tissue

In order to evaluate the wet tissue adhesive property of PNAGU and to simulate peeling under realistic conditions, the IAT of PNAGU to wet porcine skin was measured by the 90° peeling test (Fig. S6A). On one hand, PNAG and PNAGU1 display no wet skin adhesion until 30 min and 10 min, respectively. However, the other two PNAGU samples show wet skin adhesion at 5 min (Fig. S6B-E). Therefore, presence of polyurushiol segments in PNAGU hydrogel accelerate their adhesion speed to wet skin. On the other hand, IAT of PNAGU to porcine skin increases with adhesion time within 30 min. For example, that of PNAGU3 respectively increases from 20.20 to 29.95, and 37.63 J/m^2 as adhesion time prolongs from 5 to 10, and 30 min, then reaches a plateau (Fig. S6F). Obviously, PNAGU adhesive hydrogel is not an instant adhesive and the formation of adhesive bonds at the interface is a time-consuming process. These results suggest that larger content of urushiol in PNAGU hydrogel leads to higher adhesion efficiency and strength to wet tissue, i. e, PNAGU3 forms effective adhesion within 5 min and shows the largest IAT. The adhesion performance of the adhesive to wet tissue is related to its ability to break the IHL and to the interaction between adhesive groups and substrate

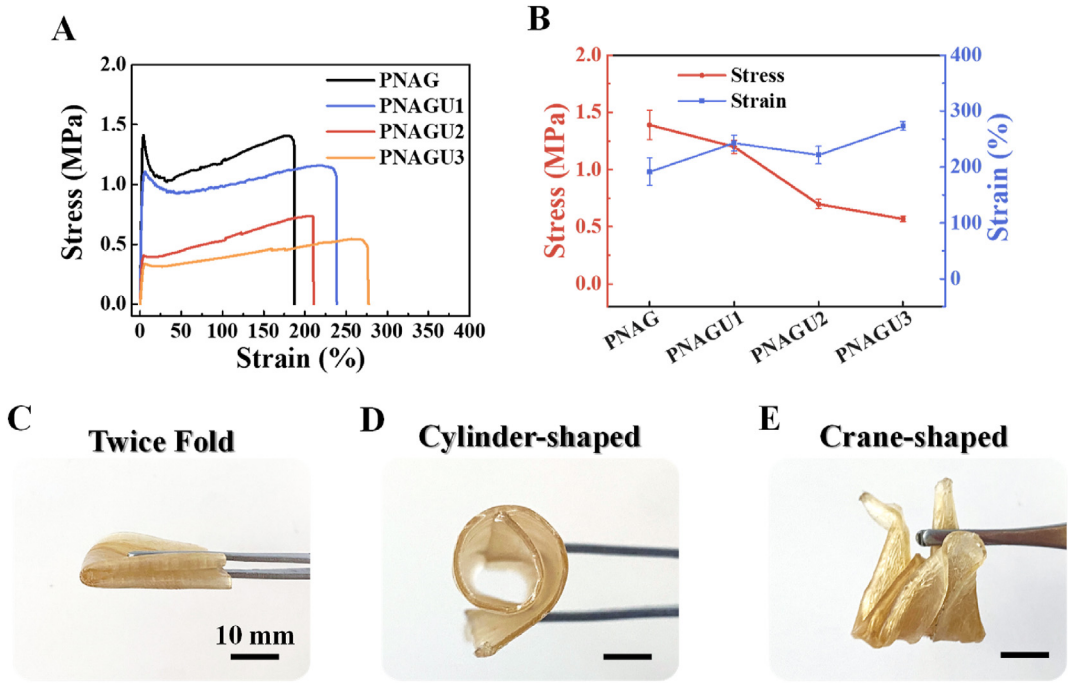

Fig. 2. Effect of urushiol content on the stress and strain of PNAGU. A) Typical stress-strain curves. B) Tensile stress and strain at break of PNAGU. PNAGU3 was C) folded twice, D) rolled, and E) folded into a crane shape.

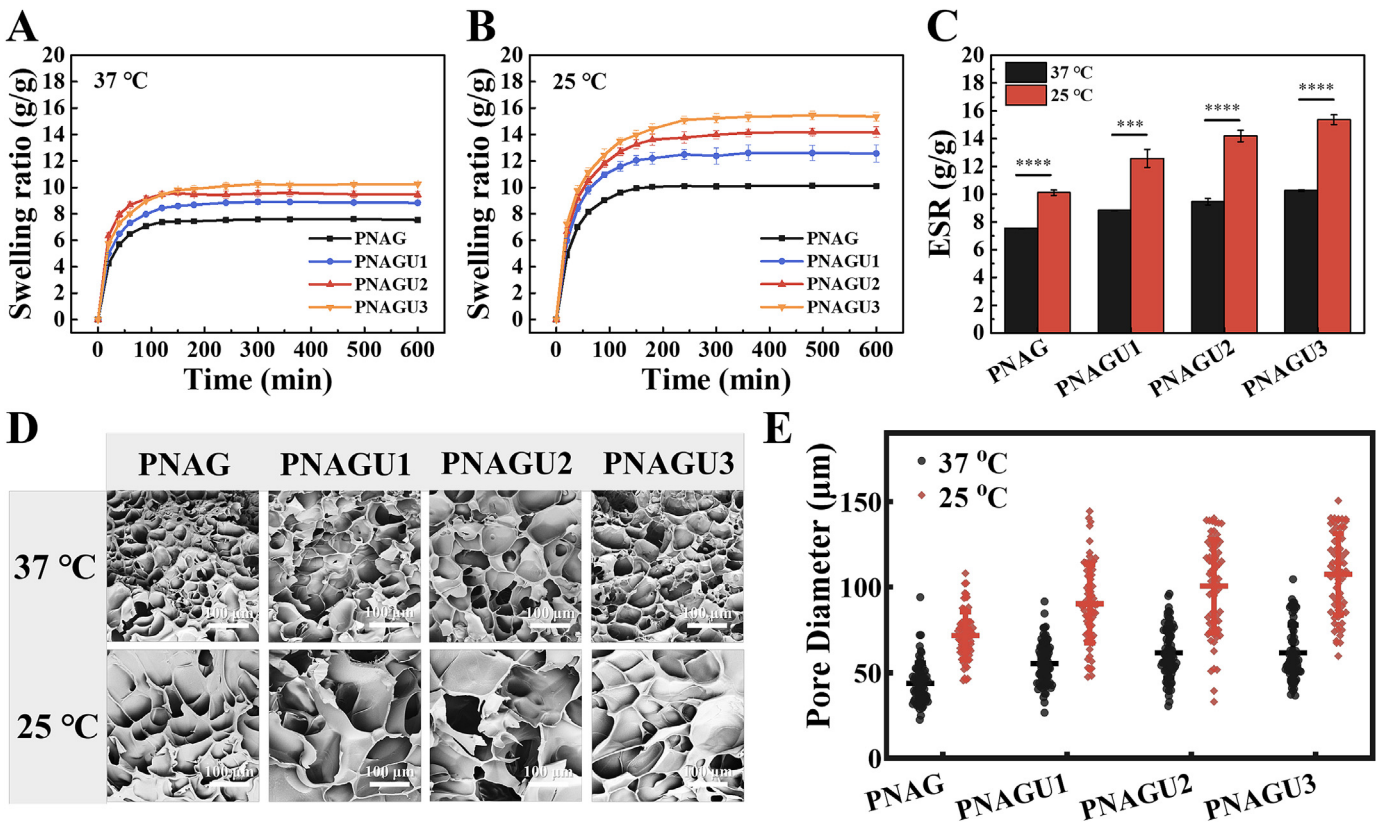

Fig. 3. Swelling and morphology of PNAGU hydrogels. Swelling performance at A) 37 °C and B) 25 °C. C) ESR at 37 °C and 25 °C. D) Cross-sectional SEM images of hydrogels at 37 °C and 25 °C, E) pore size distribution of PNAGU hydrogel at 37 °C and 25 °C. ***$p < 0.001$, ****$p < 0.0001$.

surface [2]. PNAGU can absorb the interfacial water of the wet porcine skin rapidly, meanwhile, the catechol and $-NH_3^+$ are able to break IHL, then form adhesive bonds including hydrogen bonds and cation-π interactions between hydrogel's catechol groups and functional groups on skin surface (Fig. S6G). In order to visually demonstrate the adhesion of PNAGU to wet tissue, PNAGU3 is adhered to wet porcine skin at 37 °C for 5 min, then the skin is rolled up into a cylindrical shape. Film separation from skin doesn't occur in this process, suggesting good adhesion and adaption to tissue deformation (Fig. S6H). The durability of PNAGU3 can last at least 200 days, as proved by the fact that IAT of PNAGU3 (stored in a sealed bag for more than 200 days at ambient conditions) is 34.7 J/m^2 on wet porcine skin. This is comparable to freshly prepared PNAGU3 (Fig. S7).

TAgels are used to bond together cut-open wound tissue, but easy on-demand detachment is highly required to avoid secondary injury and pain to patient upon dressing change [11,51]. As demonstrated above, PNAGU hydrogel shows thermo-responsive swelling behavior, which would provide a feasible way to realize water-driven on-demand detachment. In order to evaluate the thermo-responsive detachment performance of PNAGU hydrogel, the IAT was measured when water drops onto the adhesive interface. When treated with 25 and 37 °C water, IAT sharply drops, but it decreases to a large extent at 25 °C. For instance, it falls from 37.63 to 5.92 J/m^2 (25 °C) and to 13.32 J/m^2 (37 °C) for PNAGU3 (Fig. 4A–C). This suggests that the interfacial interaction is weakened by water treatment in an ambient temperature range of 25–37 °C, which is related to the phase transition temperature of PNAGU3 (~38.2 °C). Upon treatment with 25 °C water, the physical crosslinking loci formed by hydrophobic aggregation of isopropyl are interrupted, resulting in volume expansion of PNAGU hydrogel; Meanwhile, a large number of adhesion groups like carboxylic acid and catechol are hydrated. Both leads to the reduction of interfacial bonds (Fig. 4D), and therefore to achieve rapid detachment with no hydrogel residual left behind (Video S1). This water-driven detachable strategy highlights its simplicity so that it can be applied easily. In order to further prove polyNIPAM segment-attributed water-driven detachability of hydrogel, acrylic acid was used to replace NIPAM in the recipe of PNAGU3 to prepare an adhesive named PAAGU. IAT of PAAGU on wet porcine skin is 38.78 J/m^2, which decreases to 27.95 J/m^2 (28% reduction) with 25 °C water treatment (Fig. S8). In contrast, IAT of PNAGU3 drops from 37.63 to 5.92 J/m^2 (84% reduction). Hence, this demonstrates the pivotal contribution of polyNIPAM segments to the easy water-driven detachability of PNAGU.

Supplementary data related to this article can be found at https://doi.org/10.1016/j.mtbio.2022.100369.

The adhesion property of PNAGU3 was compared with other on-demand detachable TAgels (Fig. S9). Skin temperature-triggered debonding-on-demand (DoD) bistable adhesive polymers (BAPs [24]) and photo-detachable adhesive (Cell-Fe [26]) can adhere to dry tissue rather than wet tissue. The thermo-responsive injectable tannic acid primed thermally reversible adhesive (TAPTRA [30]) is a wet tissue adhesive, but its low cohesion often results in broken residuals on wound when it is peeled off. Compared to commercially available tissue adhesives and sealants (including cyanoacrylate adhesive (Histoacyl®), polyethylene-glycol (PEG) based sealant (Coseal®) and fibrin glue (Tisseel®) with IAT of less than 20 J/m^2 [2], our PNAGU3 has larger IAT of 37.63 J/m^2. Therefore, our water-driven detachable wet tissue adhesive PNAGU3 has good mechanical properties and IAT on wet tissues, which demonstrates the superiority of PNAGU3.

In order to further simulate the adhesion behavior of the hydrogel to fractured wet tissues, wound closure experiment is designed (Fig. 5A). The adhesion strength of PNAGU1, PNAGU2, and PNAGU3 to porcine skin is 2.32, 4.60, and 6.48 kPa, respectively (Fig. 5B and C). The highest adhesion strength of PNAGU3 agrees well with the IAT test.

Wound closure test on porcine viscera is also performed with

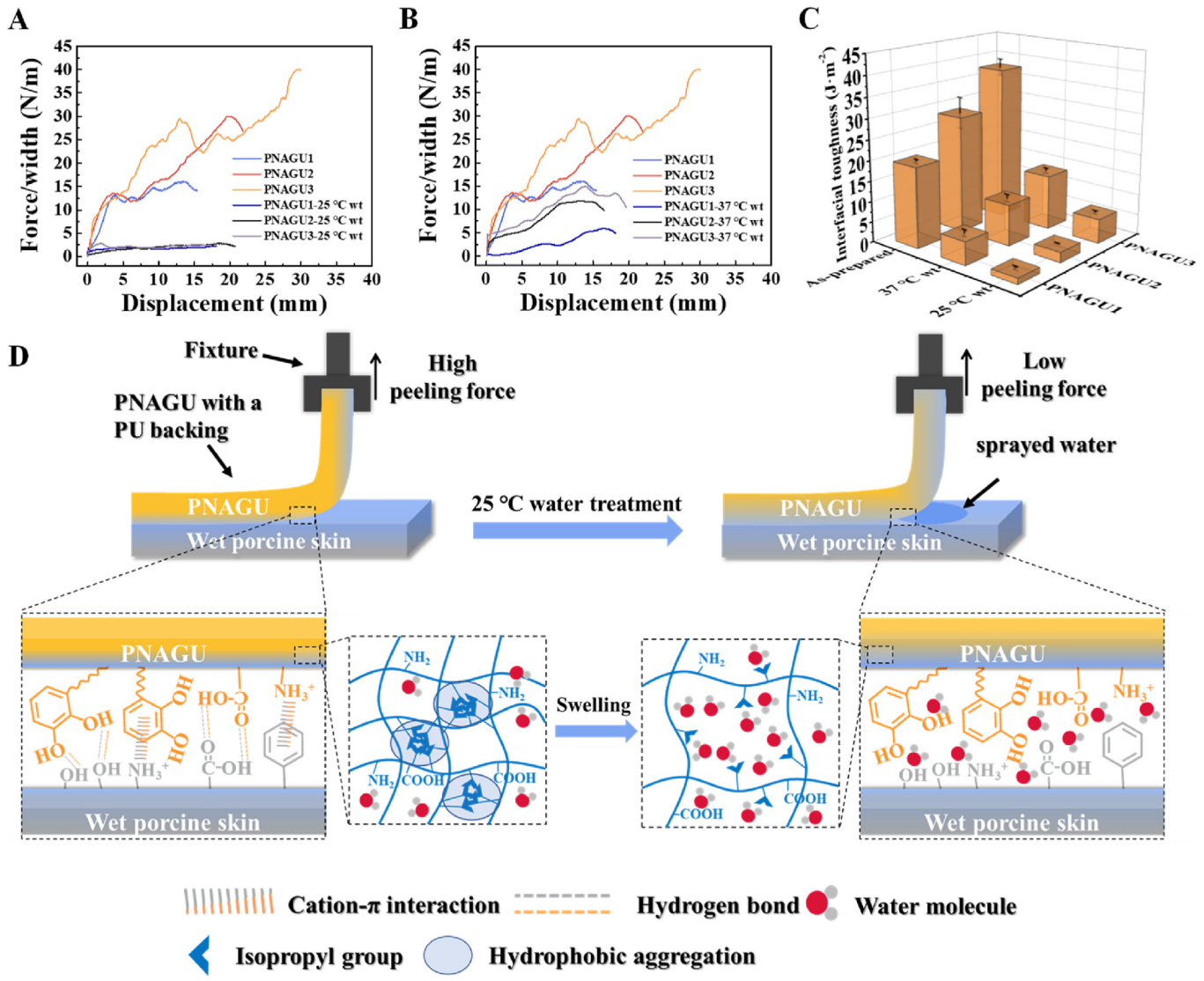

Fig. 4. Effect of water treatment on debonding PNAGU from tissue. A-B) Typical peeling force-displacement curves, C) IAT of PNAGU on wet porcine skin under water treatment at 25 and 37 °C. D) Schematic diagram of IAT test of PNAGU on porcine skin, interfacial adhesive bonds, and thermo-responsive swelling of hydrogel network.

PNAGU3. The adhesion strength to porcine liver, kidney and heart is 11.05, 7.96, and 5.36 kPa, respectively (Fig. 5D and E). Among the four porcine tissues, PNAGU3 has the strongest adhesion to porcine liver, because liver has porous structure and the adhesion groups can easily diffuse into liver [52]. It is remarkable that the displacement distance on liver is much larger than on the other tissues (Fig. 5D), showing that it undergoes large deformation without detaching from liver tissue during stretching. The digital photos and videos of the wound closure test of PNAGU3 on liver (Fig. 5F; Video S2) are strong evidences that PNAGU3 can be stretched to a long length while the bonding maintains. Finally, the hydrogel is detached from tissue surface while without cohesion failure. Fig. 5G shows that PNAGU3 bonds the two tissues and does not detach under gravity. Therefore, PNAGU3 can provide sufficient adhesive strength for wound closure.

Supplementary data related to this article can be found at https://doi.org/10.1016/j.mtbio.2022.100369.

The bursting pressure of PNAGU3 on wet small intestine model was introduced (Fig. S10A) to evaluate its resistance to internal pressure. Fig. S10B and Video S3 show the whole process of the test. Initially, the internal pressure increases to cause small intestine to bend into a banana shape. Then adhesion fails as internal pressure reaches a point. The burst pressure of PNAGU3 on wet small intestine is 10.2 kPa (Fig. S10C), which is much higher than the central venous blood pressure (~1.2 kPa), but lower than the aortic blood pressure (~16.0 kPa). Thus, PNAGU3 can meet the need for sealing capillary and even arteriole wounds, which would make it a potential wound sealing agent for hemostasis.

Supplementary data related to this article can be found at https://doi.org/10.1016/j.mtbio.2022.100369.

3.5. *In vitro hemocompatibility and cytocompatibility*

TAgels are usually used for wound closure, and wound is most often accompanied by blood exudation, so biological tissue adhesive materials must have not only excellent adhesion properties but also excellent hemocompatibility [50]. The supernatant of PNAGU3/blood suspensions with different PNAGU3 concentrations (0.5, 1.0, 2.0, and 4.0 mg/mL) is as clear as that of negative control, while the poor hemocompatibility of the positive control Triton let solution turn red (Fig. 6A). Even at the maximum concentration of 4.0 mg/mL, the hemolysis ratio of PNAGU3 is only 1.32%, revealing its good hemocompatibility.

Cytocompatibility is vital to TAgel because it would directly attach to tissue. Viability of L929 cell is used to evaluate the cytocompatibility of

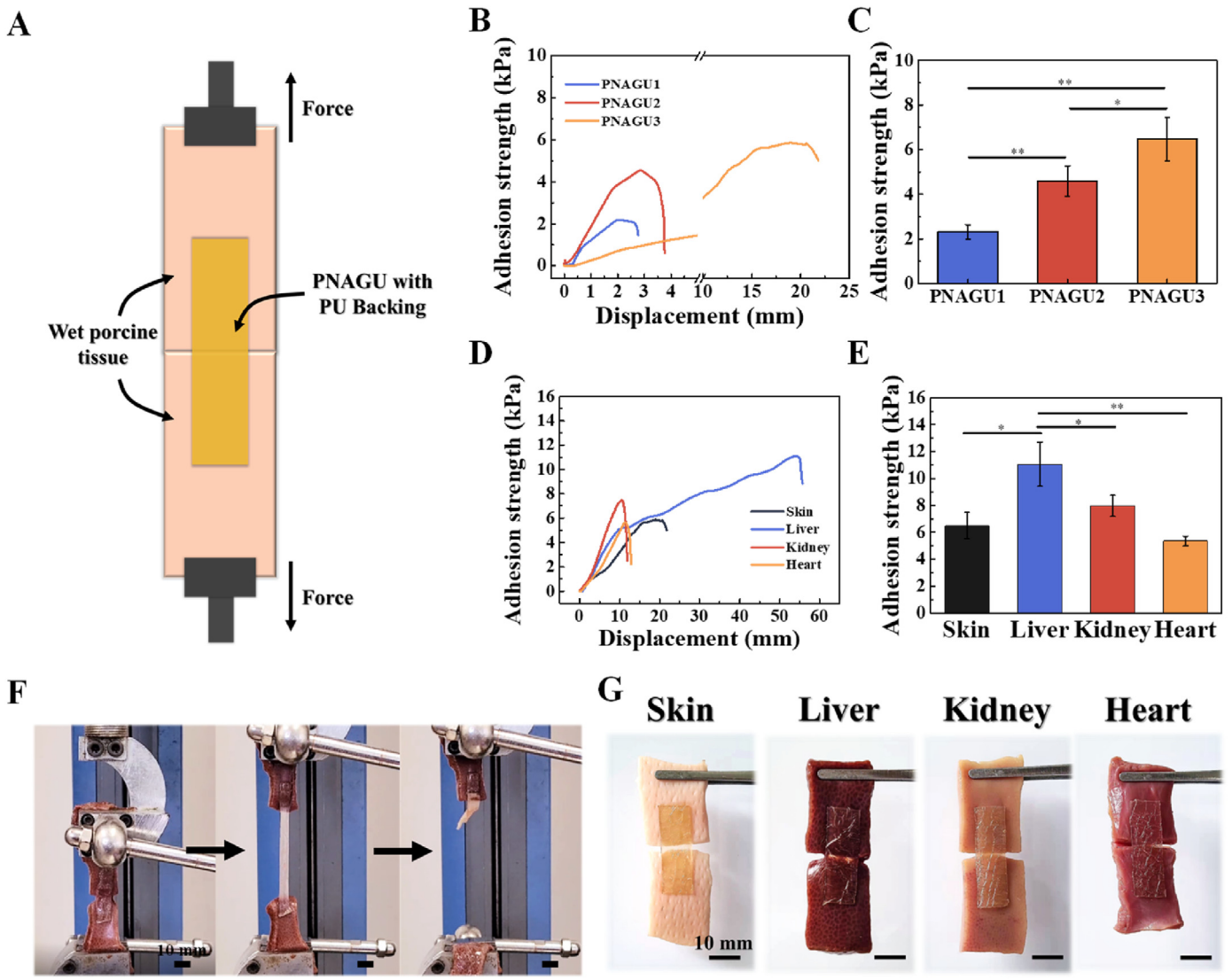

Fig. 5. A) Schematic diagram of wound closure test. B) Typical adhesion strength-displacement curves, and C) adhesion strength of PNAGU in wound closure test on wet porcine skin. D) Typical adhesion strength-displacement curves, and E) adhesion strength of PNAGU3 in wound closure tests on wet porcine skin, liver, kidney and heart. F) Digital photographs of PNAGU3 during the wound closure test on porcine liver tissue. G) Digital photographs of four different fractured tissues bonded together with PNAGU3 and lifted by a tweezer. $*p < 0.05$, $**p < 0.01$.

PNAGU3 by MTT assay. The cell viability of the extract of PNAGU3 remains >92% over 48 h incubation even with a high concentration of 50 mg/mL (Fig. 6B and C). In addition, almost all L929 cells are stained by calcein-AM (green) and with a normal shape (Fig. 6D). The cytocompatibility of PNAGU3 is also proved by proliferation of L929 cells on it, which supports that L929 cells can attach to PNAGU and maintain high viability after cultured for 2 days (Fig. S11). These results demonstrate PNAGU3 has good cytocompatibility.

3.6. *In vitro pro-coagulant property and in vivo hemostasis*

Bleeding control is of great importance for health and safety [53]. The coagulation ability of hydrogel is an important indicator for its hemostatic efficacy. BCI test is often used to evaluate the whole blood coagulation ability of hemostasis agent. The BCI value of PNAGU3 and cotton gauze is respectively 7.6% and 97.3% (Fig. 7A). It indicates that PNAGU3 has good pro-coagulant property and can accelerate the blood coagulation process, but cotton gauze can hardly facilitate the formation of blood clots. The BCI test results are in accordance with the adhesion of RBCs and platelets on the surface of PNAGU3 and cotton gauze (Fig. 7B). Only a few RBCs and platelets present on the cotton fiber surface, suggesting its poor resting ability of RBCs and platelets. In contrast, lots of RBCs and platelets stack in the pores of PNAGU3 because the good water absorption capacity of PNAGU3 enhances its ability of enriching RBCs and platelets. The long hydrophobic alkyl chains could be embedded with the hydrophobic cores of cell membranes to host RBCs and platelets [54,55]. Meanwhile, the adhesive groups of PNAGU3 facilitate the catching of RBCs and platelets. Hence, the massive aggregation of RBCs and platelets would accelerate hemostasis; Additionally, the wet tissue adhesive of PNAGU3 would contribute to the rapid formation of mechanical barriers for retarding bleeding seepage from the hydrogel/tissue interface.

When adhesive hydrogel is applied to bleeding wounds, the presence of blood may affect interfacial adhesion. IAT of PNAGU3 to porcine skin stained with rat blood at 37 °C after 30 min adhesion was tested. In this state, IAT is 40.30 J/m^2 (Fig. S12), which is near to that of PNAGU3 to wet porcine skin (37.63 J/m^2), demonstrating its good adhesion to blood-stained tissue, which would guarantee hemostasis on a bleeding wound. In vivo hemostatic ability of PNAGU3 was evaluated by rat liver injury model (Fig. 7C and D). Digital photographs of the hemostasis and detachment processes show the practical performance of PNAGU3 and

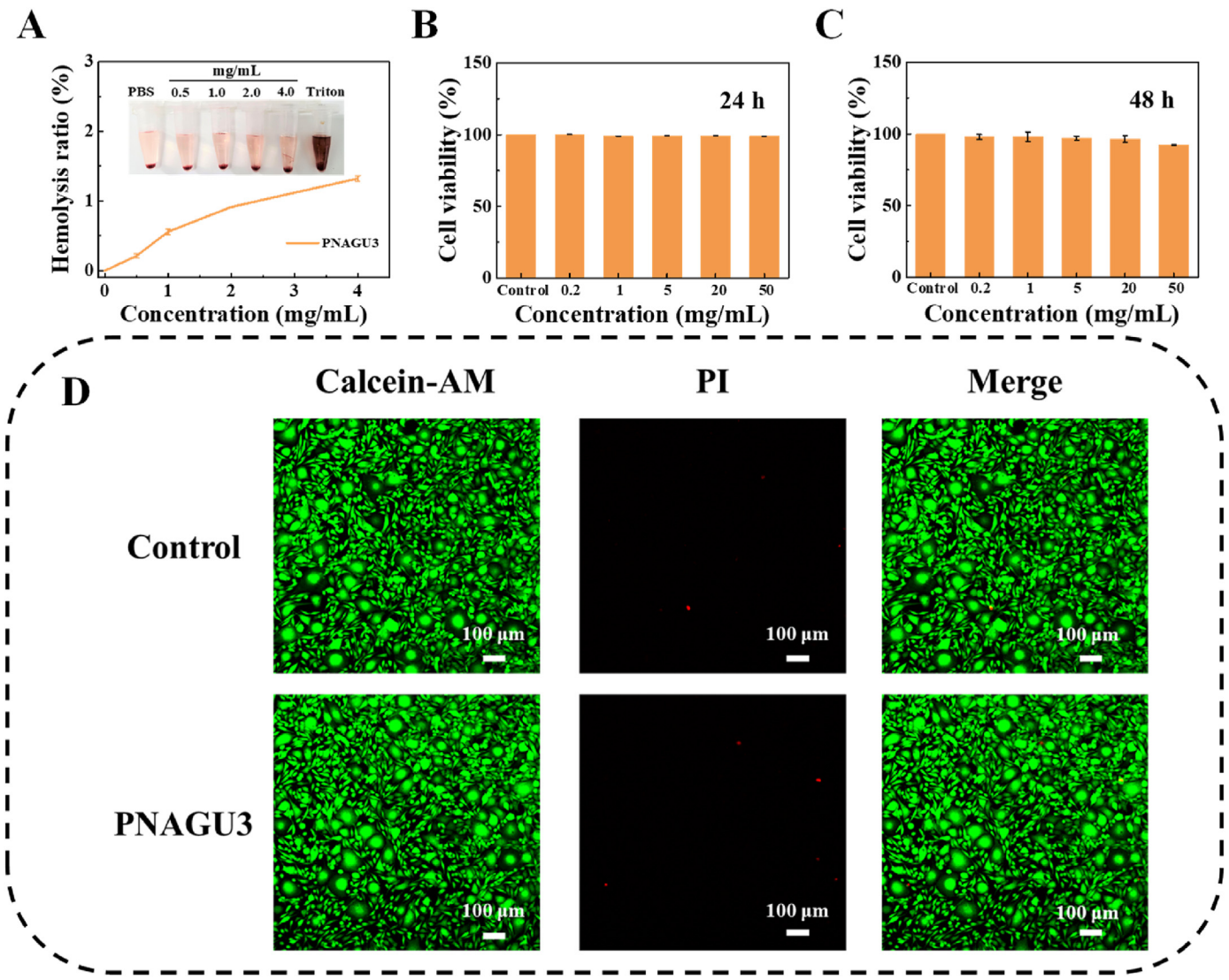

Fig. 6. A) Hemocompatibility of PNAGU3. In vitro cell viability of L929 cells cultured in the extract of PNAGU3 hydrogel at B) 24 h and C) 48 h with a concentration range of 0.2–50 mg/mL. D) Confocal laser microscopy images of L929 cells after 48 h incubation with PNAGU3.

cotton gauze. Blood quickly wetted the gauze dressing and even wetted the gauze under the liver; Blood loss gradually increased with time. In 180 s, the gauze absorbed 519 mg of blood loss, and the wound was still bleeding when the cotton gauze was removed (Video S4). This demonstrates that gauze shows a poor hemostatic efficacy in the liver injury model. In contrast, PNAGU3 could tightly adhere to rat liver without much compression, resulting in effective wound sealing, so that blood hardly seeps out and bloodstain area on the gauze does not expand in 30 s. PNAGU3 was then removed by water-driven detachment and no re-bleeding occurred (Video S5). The blood loss of PNAGU3 is only 31 mg, which is 94% lower than that of gauze (519 mg). This confirms the good hemostatic capacity of PNAGU3. Although PNAGU3 is not optically transparent (Fig. S13), the good visible light transmittance of PNAGU3 still allows user to straightforwardly visualize the state of bleeding control while sealing the bleeding site (Fig. 7E). It is important to note that directly detaching adhesive from soft tissues such as viscera may cause secondary damage to the injured [11,51], whereas PNAGU3's strategy of water-driven detachment is damage-free and harm-free.

Supplementary data related to this article can be found at https://doi.org/10.1016/j.mtbio.2022.100369.

The hemostatic mechanism of PNAGU3 is shown in Fig. 7F. First, the IHL is destroyed by quick water absorption of the hydrogel. In the meantime, the interfacial bonding formed between PNAGU3 and tissue acts as a robust barrier to seal the bleeding wounds. And Ca^{2+} released from the hydrogel activates blood clotting factors that induces the formation of fibrin [56], which constitutes the cross-linking network of thrombus. The hydrophobic chains of polyurushiol units catch RBCs and platelets via hydrophobic association, which contribute to blood gelation [55,57]. These Synergic effects of wound sealing, calcium ion-activated coagulation, and blood cells enrichment devote to rapid hemostasis to PNAGU3.

4. Conclusions

Water-driven noninvasively detachable wet tissue adhesive PNAGU hydrogels were designed and prepared by copolymerization of NIPAM, AAm, GelMA, and urushiol. In the copolymer hydrogel, catechol groups of polyurushiol units render wet tissue adhesion capability while poly-NIPAM segments impart thermo-responsive swelling-deswelling behavior. PNAGU acts as good wet tissue adhesive at human body temperature (~37 °C), and possess excellent hemocompatibility, cytocompatibility, pro-coagulant, and in vivo hemostasis efficiency. Furthermore, it is endowed with water-driven noninvasively detachment (e.g., IAT of PNAGU3 to wet porcine skin drops from 37.63 to 5.92 J/m^2

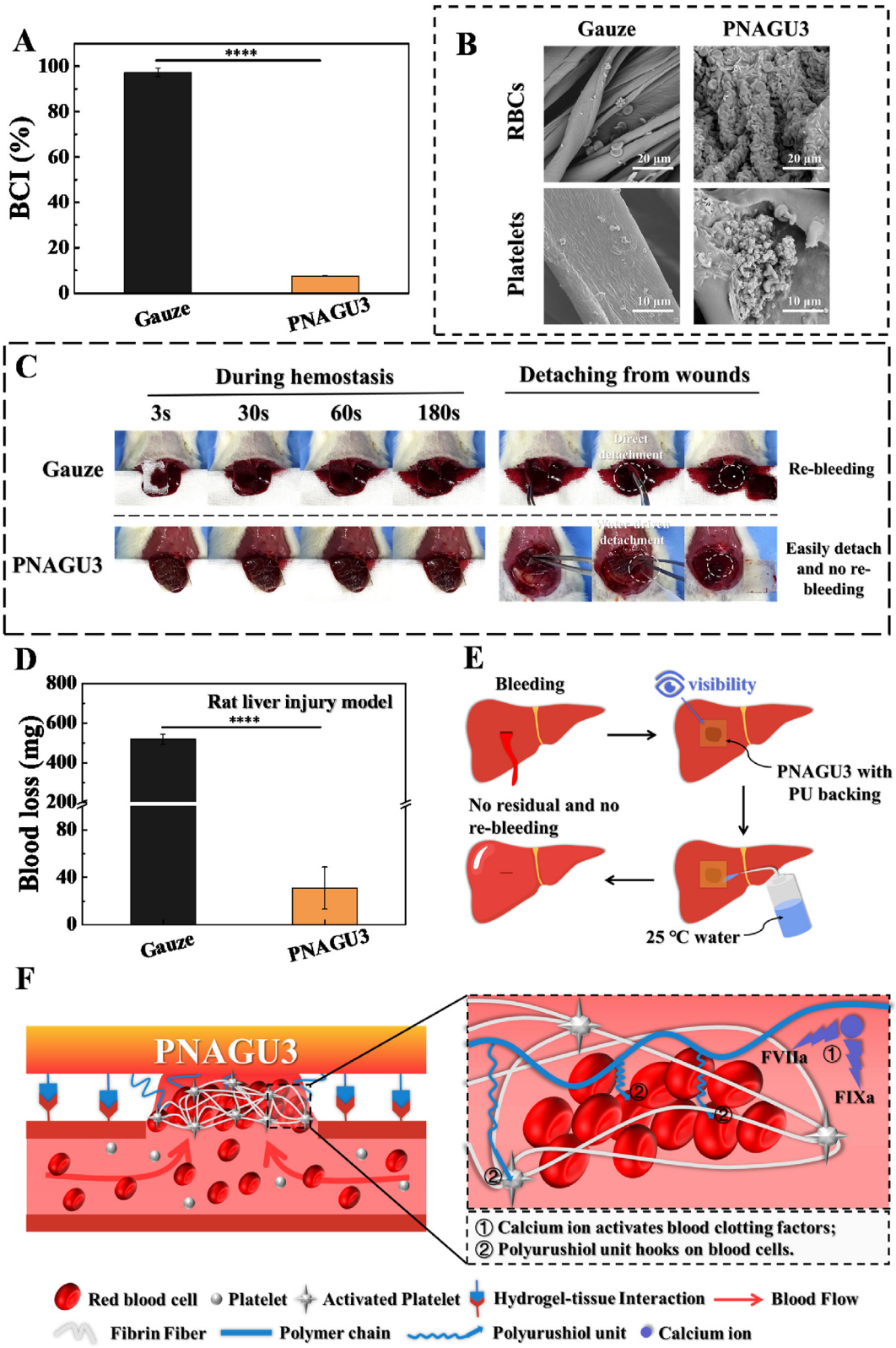

Fig. 7. A) in vitro BCI of hemostats. B) SEM images of RBCs and platelets adhesion on hemostats. C) Digital photographs of hemostasis process and detachment from the wounds. D) Blood loss in the rat liver injury model. E) Schematic diagram of the hemostasis and detachment process. F) Diagram of the hemostatic mechanism of PNAGU3. ****$p < 0.0001$.

when treated with 25 °C water). Therefore, this work provides a novel strategy for advancing the development of patient-friendly on-demand detachable w-TAgel.

Creadit author statement

H. Liu conceived and directed the project. H. Huang, P. Ni, C. Sun, H. He, X. Wang, L. Zhang and Z. Liang designed and performed the synthesis, characterization, mechanical property, tissue adhesion and hemostatic measurements of hydrogels. R. Xu and Z. Zhang carried out the tests of biocompatibility. H. Liu and H. Huang wrote the manuscript.

Data availability statement

The raw/processed data required to reproduce these findings cannot be shared at this time due to technical or time limitations.

Declaration of competing interest

The authors declare that they have no known competing financial interests or personal relationships that could have appeared to influence the work reported in this paper.

Acknowledgements

This work is supported by Natural Science Foundation of China (52103108, 22175037), Social Development of Instructive Program of Fujian Province (2020Y0020), Key Project for Advancing Science and Technology of Fujian Province ([2021]415-2021G02005), Program for Innovative Research Team in Science and Technology in Fujian Province University. Project for Undergraduate Teaching Reform in Fujian Normal University (I202002023).

Appendix A. Supplementary data

Supplementary data to this article can be found online at https://doi.org/10.1016/j.mtbio.2022.100369.

References

[1] A.D.C.J. Li, J. Yang, Q. Yang, Z. Suo, D.J. Mooney, Tough adhesives for diverse wet surfaces, Science 357 (2017) 378–381.
[2] H. Yuk, C.E. Varela, C.S. Nabzdyk, X. Mao, R.F. Padera, E.T. Roche, X. Zhao, Dry double-sided tape for adhesion of wet tissues and devices, Nature 575 (2019) 169–174.
[3] X. Du, Y. Liu, H. Yan, M. Rafique, S. Li, X. Shan, L. Wu, M. Qiao, D. Kong, L. Wang, Anti-infective and pro-coagulant chitosan-based hydrogel tissue adhesive for sutureless wound closure, Biomacromolecules 21 (2020) 1243–1253.
[4] S. Li, N. Chen, X. Li, Y. Li, Z. Xie, Z. Ma, J. Zhao, X. Hou, X. Yuan, Bioinspired double-dynamic-bond crosslinked bioadhesive enables post-wound closure care, Adv. Funct. Mater. 30 (2020), 2000130.
[5] X. Zhao, D. Pei, Y. Yang, K. Xu, J. Yu, Y. Zhang, Q. Zhang, G. He, Y. Zhang, A. Li, Y. Cheng, X. Chen, Green tea derivative driven smart hydrogels with desired functions for chronic diabetic wound treatment, Adv. Funct. Mater. 31 (2021), 2009442.
[6] Y. Wang, F. Huang, X. Chen, X.-W. Wang, W.-B. Zhang, J. Peng, J. Li, M. Zhai, Stretchable, conductive, and self-healing hydrogel with super metal adhesion, Chem. Mater. 30 (2018) 4289–4297.
[7] D. Zhang, Y. Tang, Y. Zhang, F. Yang, Y. Liu, X. Wang, J. Yang, X. Gong, J. Zheng, Highly stretchable, self-adhesive, biocompatible, conductive hydrogels as fully polymeric strain sensors, J. Mater. Chem. 8 (2020) 20474–20485.
[8] D.W. Kim, K.I. Song, D. Seong, Y.S. Lee, S. Baik, J.H. Song, H.J. Lee, D. Son, C. Pang, Electrostatic-mechanical synergistic in situ multiscale tissue adhesion for sustainable residue-free bioelectronics interfaces, Adv. Mater. (2021), 2105338.
[9] S. Li, Y. Cong, J. Fu, Tissue adhesive hydrogel bioelectronics, J. Mater. Chem. B 9 (2021) 4423–4443.
[10] W. Zhang, R. Wang, Z. Sun, X. Zhu, Q. Zhao, T. Zhang, A. Cholewinski, F.K. Yang, B. Zhao, R. Pinnaratip, P.K. Forooshani, B.P. Lee, Catechol-functionalized hydrogels: biomimetic design, adhesion mechanism, and biomedical applications, Chem. Soc. Rev. 49 (2020) 433–464.
[11] Y. Zhang, T.H. Tao, Skin-friendly electronics for acquiring human physiological signatures, Adv. Mater. 31 (2019), 1905767.
[12] R. Michel, L. Poirier, Q. van Poelvoorde, J. Legagneux, M. Manassero, L. Corte, Interfacial fluid transport is a key to hydrogel bioadhesion, Proc. Natl. Acad. Sci. U.S.A. 116 (2019) 738–743.
[13] X. Mao, H. Yuk, X. Zhao, Hydration and swelling of dry polymers for wet adhesion, J. Mech. Phys. Solid. 137 (2020), 103863.
[14] Q. Guo, J. Chen, J. Wang, H. Zeng, J. Yu, Recent progress in synthesis and application of mussel-inspired adhesives, Nanoscale 12 (2020) 1307–1324.
[15] Y. Chen, Y. Qiu, Q. Wang, D. Li, T. Hussain, H. Ke, Q. Wei, Mussel-inspired sandwich-like nanofibers/hydrogel composite with super adhesive, sustained drug release and anti-infection capacity, Chem. Eng. J. 399 (2020), 125668.
[16] H. Fan, J. Wang, J.P. Gong, Barnacle cement proteins-inspired tough hydrogels with robust, long-lasting, and repeatable underwater adhesion, Adv. Funct. Mater. 31 (2020), 2009334.
[17] X. Su, Y. Luo, Z. Tian, Z. Yuan, Y. Han, R. Dong, L. Xu, Y. Feng, X. Liu, J. Huang, Ctenophore-inspired hydrogels for efficient and repeatable underwater specific adhesion to biotic surfaces, Mater. Horiz. 7 (2020) 2651–2661.
[18] T.M. Lutz, C. Kimna, A. Casini, O. Lieleg, Bio-based and bio-inspired adhesives from animals and plants for biomedical applications, Mater. Today Bio 13 (2022), 100203.
[19] Y. Akdogan, W. Wei, K.-Y. Huang, Y. Kageyama, E.W. Danner, D.R. Miller, N.R. Martinez Rodriguez, J.H. Waite, S. Han, Intrinsic surface-drying properties of bioadhesive proteins, Angew. Chem. Int. Ed. 53 (2014) 11253–11256.
[20] J. Saiz-Poseu, J. Mancebo-Aracil, F. Nador, F. Busque, D. Ruiz-Molina, The chemistry behind catechol-based adhesion, Angew. Chem. Int. Ed. 58 (2019) 696–714.
[21] Y. Gao, K. Wu, Z. Suo, Photodetachable adhesion, Adv. Mater. 31 (2019), 1806948.
[22] X. Chen, H. Yuk, J. Wu, C.S. Nabzdyk, X. Zhao, Instant tough bioadhesive with triggerable benign detachment, Proc. Natl. Acad. Sci. U.S.A. 117 (2020) 15497–15503.
[23] K. Chen, Q. Lin, L. Wang, Z. Zhuang, Y. Zhang, D. Huang, H. Wang, An all-in-one tannic acid-containing hydrogel adhesive with high toughness, notch insensitivity, self-healability, tailorable topography, and strong, instant, and on-demand underwater adhesion, ACS Appl. Mater. Interfaces 13 (2021) 9748–9761.
[24] M. Gao, H. Wu, R. Plamthottam, Z. Xie, Y. Liu, J. Hu, S. Wu, L. Wu, X. He, Q. Pei, Skin temperature-triggered, debonding-on-demand sticker for a self-powered mechanosensitive communication system, Matter 4 (2021) 1962–1974.
[25] T. Hendrickson, C. Lupo, G. Bauza, L. Tavares, S. Ingram, S. Wang, M. Moreno, E. Tasciotti, M. Valderrabano, F. Taraballi, Thermally responsive hydrogel for atrial fibrillation related stroke prevention, Mater. Today Bio 14 (2022), 100240.
[26] M. Jiang, X. Liu, Z. Chen, J. Li, S. Liu, S. Li, Near-infrared-detached adhesion enabled by upconverting nanoparticles, iScience 23 (2020), 100832.
[27] G. Xu, L. Cheng, Q. Zhang, Y. Sun, C. Chen, H. Xu, Y. Chai, M. Lang, In situ thiolated alginate hydrogel: instant formation and its application in hemostasis, J. Biomater. Appl. 31 (2016) 721–729.
[28] M. Dompe, F.J. Cedano-Serrano, O. Heckert, N. van den Heuvel, J. van der Gucht, Y. Tran, D. Hourdet, C. Creton, M. Kamperman, Thermoresponsive complex coacervate-based underwater adhesive, Adv. Mater. 31 (2019), 1808179.
[29] X. Shi, P. Wu, A smart patch with on-demand detachable adhesion for bioelectronics, Small 17 (2021), 2101220.
[30] B. Li, J.J. Whalen, M.S. Humayun, M.E. Thompson, Reversible bioadhesives using tannic acid primed thermally-responsive polymers, Adv. Funct. Mater. 30 (2019), 1907478.
[31] H. He, W. Zhou, J. Gao, F. Wang, S. Wang, Y. Fang, Y. Gao, W. Chen, W. Zhang, Y. Weng, Z. Wang, H. Liu, Efficient, biosafe and tissue adhesive hemostatic cotton gauze with controlled balance of hydrophilicity and hydrophobicity, Nat. Commun. 13 (2022) 552.
[32] X. Fan, W. Zhou, Y. Chen, L. Yan, Y. Fang, H. Liu, An antifreezing/antiheating hydrogel containing catechol derivative urushiol for strong wet adhesion to various substrates, ACS Appl. Mater. Interfaces 12 (2020) 32031–32040.
[33] Y. Ono, T. Shikata, Contrary hydration behavior of N-isopropylacrylamide to its polymer, P(NIPAm), with a lower critical solution temperature, J. Phys. Chem. B 111 (2007) 1511–1513.
[34] D.C. Leite, S. Kakorin, Y. Hertle, T. Hellweg, N.P. da Silveira, Smart starch-poly(N-isopropylacrylamide) hybrid microgels: synthesis, structure, and swelling behavior, Langmuir 34 (2018) 10943–10954.
[35] Z. Li, S. Zhang, Y. Chen, H. Ling, L. Zhao, G. Luo, X. Wang, M.C. Hartel, H. Liu, Y. Xue, R. Haghniaz, K. Lee, W. Sun, H. Kim, J. Lee, Y. Zhao, Y. Zhao, S. Emaminejad, S. Ahadian, N. Ashammakhi, M.R. Dokmeci, Z. Jiang, A. Khademhosseini, Gelatin methacryloyl-based tactile sensors for medical wearables, Adv. Funct. Mater. 30 (2020), 2003601.
[36] A. Assmann, A. Vegh, M. Ghasemi-Rad, S. Bagherifard, G. Cheng, E.S. Sani, G.U. Ruiz-Esparza, I. Noshadi, A.D. Lassaletta, S. Gangadharan, A. Tamayol, A. Khademhosseini, N. Annabi, A highly adhesive and naturally derived sealant, Biomaterials 140 (2017) 115–127.
[37] H. Montazerian, A. Baidya, R. Haghniaz, E. Davoodi, S. Ahadian, N. Annabi, A. Khademhosseini, P.S. Weiss, Stretchable and bioadhesive gelatin methacryloyl-based hydrogels enabled by in situ dopamine polymerization, ACS Appl. Mater. Interfaces 13 (2021) 40290–40301.
[38] M.C. Chang, C.-C. Ko, W.H. Douglas, Preparation of hydroxyapatite-gelatin nanocomposite, Biomaterials 24 (2003) 2853–2862.
[39] S. Xu, D. Sheng, X. Liu, F. Ji, Y. Zhou, L. Dong, H. Wu, Y. Yang, A seawater-assisted self-healing metal–catechol polyurethane with tunable mechanical properties, Polym. Int. 68 (2019) 1084–1090.
[40] W.D. Bush, J.D. Simon, Quantification of Ca(2+) binding to melanin supports the hypothesis that melanosomes serve a functional role in regulating calcium homeostasis, Pigm. Cell Res. 20 (2007) 134–139.

[41] J. Li, H. Ejima, N. Yoshie, Seawater-Assisted self-healing of catechol polymers via hydrogen bonding and coordination interactions, ACS Appl. Mater. Interfaces 8 (2016) 19047–19053.
[42] H. Shirahama, B.H. Lee, L.P. Tan, N.J. Cho, Precise tuning of facile one-pot gelatin methacryloyl (GelMA) synthesis, Sci. Rep. 6 (2016), 31036.
[43] J.-P. Chen, T.-F. Yang, Applications of chitosan-based thermo-sensitive copolymers for harvesting living cell sheet, Appl. Surf. Sci. 255 (2008) 297–300.
[44] X. Fan, Y. Fang, W. Zhou, L. Yan, Y. Xu, H. Zhu, H. Liu, Mussel foot protein inspired tough tissue-selective underwater adhesive hydrogel, Mater. Horiz. 8 (2021) 997–1007.
[45] B. Lee, H. Han, H.G. Hahn, J.M. Doh, S.H. Park, E. Lee, S.S. Lee, C. Park, H.S. Lim, J.A. Lim, Ecofriendly catechol lipid bioresin for low-temperature processed electrode patterns with strong durability, ACS Appl. Mater. Interfaces 12 (2020) 16864–16876.
[46] X. Lin, Y. Mao, P. Li, Y. Bai, T. Chen, K. Wu, D. Chen, H. Yang, L. Yang, Ultra-conformable ionic skin with multi-modal sensing, broad-spectrum antimicrobial and regenerative capabilities for smart and expedited wound care, Adv. Sci. 8 (2021), 2004627.
[47] X. Yang, W. Liu, N. Li, M. Wang, B. Liang, I. Ullah, A. Luis Neve, Y. Feng, H. Chen, C. Shi, Design and development of polysaccharide hemostatic materials and their hemostatic mechanism, Biomater. Sci. 5 (2017) 2357–2368.
[48] R. Lv, Z. Bei, Y. Huang, Y. Chen, Z. Zheng, Q. You, C. Zhu, Y. Cao, Mussel-Inspired flexible, wearable, and self-adhesive conductive hydrogels for strain sensors, Macromol. Rapid Commun. 41 (2020), 1900450.
[49] L. Fischer, A.K. Strzelczyk, N. Wedler, C. Kropf, S. Schmidt, L. Hartmann, Sequence-defined positioning of amine and amide residues to control catechol driven wet adhesion, Chem. Sci. 11 (2020) 9919–9924.
[50] M. Li, Y. Liang, J. He, H. Zhang, B. Guo, Two-pronged strategy of biomechanically active and biochemically multifunctional hydrogel wound dressing to accelerate wound closure and wound healing, Chem. Mater. 32 (2020) 9937–9953.
[51] Z. Li, A. Milionis, Y. Zheng, M. Yee, L. Codispoti, F. Tan, D. Poulikakos, C.H. Yap, Superhydrophobic hemostatic nanofiber composites for fast clotting and minimal adhesion, Nat. Commun. 10 (2019) 5562.
[52] S. Lorente, M. Hautefeuille, A. Sanchez-Cedillo, The liver, a functionalized vascular structure, Sci. Rep. 10 (2020), 16194.
[53] Z. Ni, H. Yu, L. Wang, X. Liu, D. Shen, X. Chen, J. Liu, N. Wang, Y. Huang, Y. Sheng, Polyphosphazene and non-catechol-based antibacterial injectable hydrogel for adhesion of wet tissues as wound dressing, Adv. Healthc. Mater. 11 (2021), 2101421.
[54] M.B. Dowling, R. Kumar, M.A. Keibler, J.R. Hess, G.V. Bochicchio, S.R. Raghavan, A self-assembling hydrophobically modified chitosan capable of reversible hemostatic action, Biomaterials 32 (2011) 3351–3357.
[55] G. Chen, Y. Yu, X. Wu, G. Wang, J. Ren, Y. Zhao, Bioinspired multifunctional hybrid hydrogel promotes wound healing, Adv. Funct. Mater. 28 (2018), 1801386.
[56] M.N. Sundaram, U. Mony, P.K. Varma, J. Rangasamy, Vasoconstrictor and coagulation activator entrapped chitosan based composite hydrogel for rapid bleeding control, Carbohydr. Polym. 258 (2021), 117634.
[57] C. Cui, C. Fan, Y. Wu, M. Xiao, T. Wu, D. Zhang, X. Chen, B. Liu, Z. Xu, B. Qu, W. Liu, Water-triggered hyperbranched polymer universal adhesives: from strong underwater adhesion to rapid sealing hemostasis, Adv. Mater. 31 (2019), 1905761.